Monthly Notices of the ROYAL ASTRONOMICAL SOCIETY

Mon. Not. R. Astron. Soc. **415,** 854–866 (2011) doi:10.1111/j.1365-2966.2011.18765.x

The Volume-limited A-Star (VAST) survey – I. Companions and the unexpected X-ray detection of B6–A7 stars

R. J. De Rosa,[1⋆] J. Bulger,[1] J. Patience,[1,2] B. Leland,[1] B. Macintosh,[2] A. Schneider,[3] I. Song,[3] C. Marois,[4] J. R. Graham,[5,6] M. Bessell[7] and R. Doyon[8]

[1]*School of Physics, Exeter University, Stocker Road, Exeter EX4 4QL*
[2]*Institute of Geophysics and Planetary Physics, Lawrence Livermore National Laboratory, 7000 East Avenue, Livermore, CA 94550, USA*
[3]*Physics and Astronomy, University of Georgia, 240 Physics, Athens, GA 30602, USA*
[4]*NRC Herzberg Institute of Astrophysics, 5071 West Saanich Road, Victoria, BC V9E 2E7, Canada*
[5]*Astronomy Department, University of California, Berkeley, CA 94720, USA*
[6]*Dunlap Institute for Astronomy and Astrophysics, University of Toronto, 50 St George Street, Toronto, ON M55 3H8, Canada*
[7]*Mount Stromlo and Siding Spring Observatories, Institute of Advanced Studies, The Australian National University, Weston Creek PO, ACT 2611, Australia*
[8]*Dépt de Physique, Université de Montréal, C.P. 6128, Succ. Centre-Ville, Montréal, QC H3C 3J7, Canada*

Accepted 2011 March 19. Received 2011 March 17; in original form 2010 September 24

ABSTRACT

With an adaptive optics imaging survey of 148 B6–A7 stars, we have tested the hypothesis that unresolved lower mass companions are the source of the unexpected X-ray detections of stars in this spectral type range. The sample is composed of 63 stars detected in X-rays within the *ROSAT* All Sky Survey and 85 stars that form a control sample; both subsets have the same restricted distribution of spectral type, age, X-ray sensitivity and separation coverage. A total of 68 companion candidates are resolved with separations ranging from 0.3 to 26.2 arcsec, with 23 new detections. The multiple star frequency of the X-ray sample based on companions resolved within the *ROSAT* error ellipse is found to be 43^{+6}_{-6} per cent. The corresponding control sample multiple star frequency is three times lower at 12^{+4}_{-3} per cent – a difference of 31 ± 7 per cent. These results are presented in the first of a series of papers based on our Volume-limited A-Star (VAST) survey – a comprehensive study of the multiplicity of A-type stars.

Key words: techniques: high angular resolution – binaries: general – stars: early-type – stars: imaging – X-rays: stars.

1 INTRODUCTION

The detection of X-ray emission from main-sequence stars is common (Vaiana et al. 1981), with the notable exception of late B-type and early A-type stars (e.g. Stauffer et al. 1994). Two distinct generation mechanisms are responsible for the X-ray emission, related to the different stellar structure of massive O- and B-type stars and lower mass F- to M-type stars. For the massive stars, the hot stellar winds cause X-ray emission, while the lower mass stars produce X-rays from the confinement of superheated plasma within their magnetic fields.

Radiative winds driven by line absorption and re-emission within the extended atmospheres of O-type and early B-type stars form a key component of the model for X-ray emission from these massive stars (e.g. Lucy & White 1980). Wind shocks caused either through instability generated through radiative driving (Owocki, Castor & Rybicki 1988) or due to collisions of magnetically driven wind streams (Feldmeier, Puls & Pauldrach 1997) are thought to be the primary X-ray-generation mechanisms. Interaction between stellar winds and surrounding material is also thought to produce X-rays (e.g. Giampapa, Prosser & Fleming 1998).

For lower mass stars, stellar winds are too weak to generate X-rays, and the stellar corona is responsible for the emission of X-rays and is intrinsically linked to the magnetic field. For late A-type to early M-type stars, magnetic fields arise from the $\alpha\Omega$ dynamo caused by the differential rotation at the interface between the convective envelope and the radiative core (Spiegel & Weiss 1980). The magnetic field generated by the dynamo process is essential for confining the superheated plasma necessary for X-ray generation (Güdel 2004). The heating mechanism required to maintain the corona at temperatures greater than 10^6 K was originally thought to be acoustic waves (e.g. Schwarzschild 1948; Schatzman 1949), while current models involve Alfvén waves travelling perpendicular to the magnetic field (e.g. De-Pontieu et al. 2007; Jess et al. 2009). Localized magnetic reconnection events within the chromosphere are also a potential source of coronal heating through Joule heating (e.g. Sturrock 1999). Beginning at a spectral type

⋆E-mail: derosa@astro.ex.ac.uk

of M3 ($\sim$0.35 M$_\odot$), the stars become fully convective (Chabrier & Baraffe 1997) and the high level of magnetic activity observed (e.g. Randich 2000) may be due to an α^2-type dynamo-generation mechanism (Chabrier & Küker 2006), in which turbulent motions are able to generate large-scale magnetic fields.

In addition to the emission mechanisms intrinsic to the star, X-rays can be generated by processes involving binary systems. Accretion of material within cataclysmic variable systems (e.g. Patterson & Raymond 1985) and compact object binaries (e.g. Shapiro, Lightman & Eardley 1976) can produce X-ray fluxes. For stars between spectral types B6 and A7, which are expected to be X-ray quiet, the presence of a low-mass companion can lead to the detection of X-rays which are assigned to the primary if the companion is unknown. This study is designed to explore the hypothesis that unresolved lower mass companions are the true source of the unexpected X-ray detections from B6–A7 stars.

2 PREVIOUS OBSERVATIONS

2.1 X-ray detection of B6–A7 stars

Early studies of stellar X-ray emission conducted with the *Einstein Observatory* measured a notable decrease in the fraction of X-ray-detected A-type stars ($0.00 \lesssim B - V \lesssim 0.25$) compared to bluer and redder stars (Topka et al. 1982; Schmitt et al. 1985). Out of the 35 A-type stars observed by Schmitt et al. (1985), only seven were detected and four were listed as having a secondary component which could be the source of the X-ray emission. *Einstein* observations of coeval stellar groups also showed a similar decrease in the fraction of X-ray detections of A-type stars between $0.00 \lesssim B - V \lesssim 0.3$ (e.g. Micela et al. 1985; Schmitt et al. 1990).

The increased sensitivity provided by the *ROSAT* mission and all-sky coverage led to the detection and characterization of a significant number of stellar X-ray sources (Voges et al. 1999). A search by Huensch, Schmitt & Voges (1998b) of the Bright Star Catalogue (Hoffleit 1969) and the *ROSAT* Bright Source Catalogue (BSC) for objects within 90 arcsec of the same position defined a population of 232 B6–A7 X-ray-detected stars. To investigate possible sources of the X-ray emission for this sample, the X-ray luminosity was compared with spectral type, spectral peculiarities and rotational velocities (e.g. Simon, Drake & Kim 1995; Schröder & Schmitt 2007). The lack of a dependence on any of these factors was taken as evidence of unresolved companions. Without a comprehensive binary survey of A-type stars, it was not possible to test the companion hypothesis directly. Similarly, X-ray data from *Chandra*, which could resolve the emission source in tight ($\rho \sim$ 0.5 arcsec) binary systems, do not exist for a significant sample of X-ray B6–A7 stars.

2.2 High-resolution imaging companion searches

High-resolution adaptive optics (AO) imaging studies of X-ray-detected B- and A-type stars have been employed to search for lower mass stars capable of producing X-rays. Pointed observations of late B-type stars with known lower mass companions (e.g. Schmitt et al. 1993; Berghofer & Schmitt 1994) wide enough to be resolved with the *ROSAT* High Resolution Imager were obtained to determine the source of the X-ray emission. These observations typically identified the B-type star as the source of X-ray emission, although subsequent high-resolution AO imaging has revealed additional components to several of these systems (e.g. Shatsky & Tokovinin 2002). Subarcsecond binary companions have also been resolved with high-resolution AO imaging of pre-main-sequence companions to late B-type stars (e.g. Hubrig et al. 2001).

Recent discoveries of low-mass companions to Alcor (Mamajek et al. 2010; Zimmerman et al. 2010) and ζ Virginis (Hinkley et al. 2010) have both noted that the unexplained X-ray emission from the primary can be explained by the lower mass companion, and demonstrated how X-ray emission from A-type stars could be a useful tool in searching for low-mass companions. The current study expands upon the existing imaging results of X-ray-detected B6–A7 stars by observing a large sample of both X-ray stars and a control sample.

3 SAMPLE

Two samples were constructed in order to test the companion hypothesis: a 63-star X-ray-detected sample and an 85-star control sample. The distributions of spectral types reported in the *Hipparcos* catalogue (ESA 1997) for both samples are shown in Fig. 1, and a Kolmogorov–Smirnov (KS) test confirms that both are drawn from the same distribution. The majority of the total sample, 108 targets, form a part of our ongoing Volume-limited A-Star (VAST) survey which will include all A-type stars within 75 pc. Both the X-ray and control samples include targets spanning a similar range of ages, as shown in the colour–magnitude diagram in Fig. 2. To perform a robust test of the companion hypothesis, we ensured that each sample had a similar distribution of sensitivity to X-ray sources. Background X-ray counts were extracted from the *ROSAT* All Sky Survey (RASS) observations at the coordinates of each target within both samples. A minimum detectable X-ray flux at each coordinate was estimated as five times the background level. These minimum fluxes were calculated assuming a hardness ratio of 0.5, typical of low-mass stellar sources (e.g. Huélamo et al. 2000). The X-ray luminosity (L_X) was then calculated based on a distance equal to that of the target. The distributions of minimum detectable L_X for both samples are shown in Fig. 3.

The latest spectral type companion to which the RASS observations are sensitive depends on the age of the target, derived from theoretical isochrones (Fig. 2; Marigo et al. 2008), and the X-ray luminosity sensitivity of the observations (Fig. 3). The distribution of this spectral type sensitivity is given in Fig. 4. Most of the targets within both samples had RASS observations sensitive to M-type

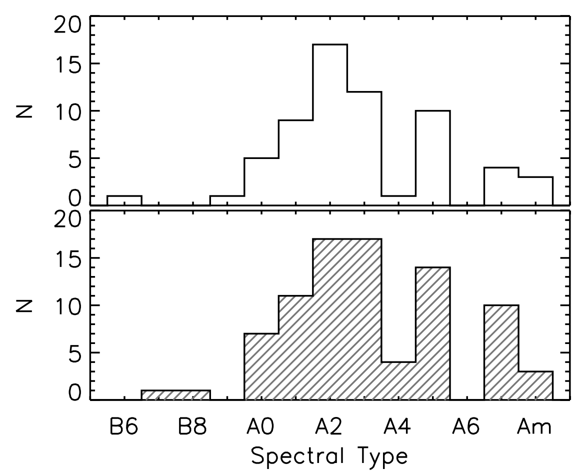

Figure 1. Distribution of the spectral type for each target reported within the *Hipparcos* catalogue for the X-ray (white histogram) and control (grey histogram) samples.

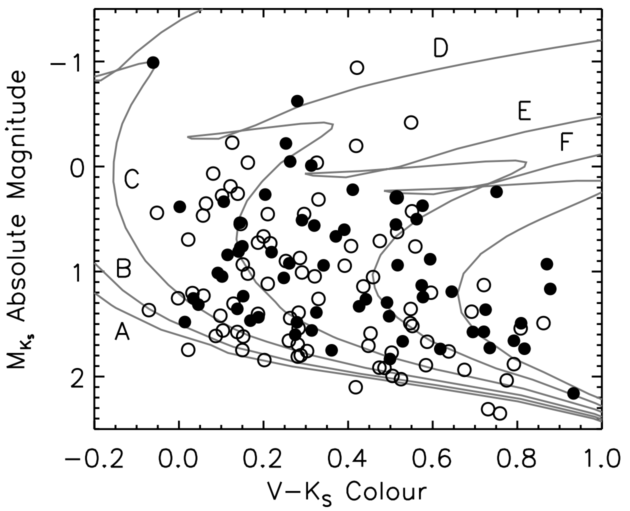

Figure 2. A colour–magnitude diagram of the X-ray (filled circles) and control (open circles) samples. Theoretical isochrones are plotted for A – 10 Myr, B – 100 Myr, C – 250 Myr, D – 500 Myr, E – 800 Myr and F – 1 Gyr (Marigo et al. 2008).

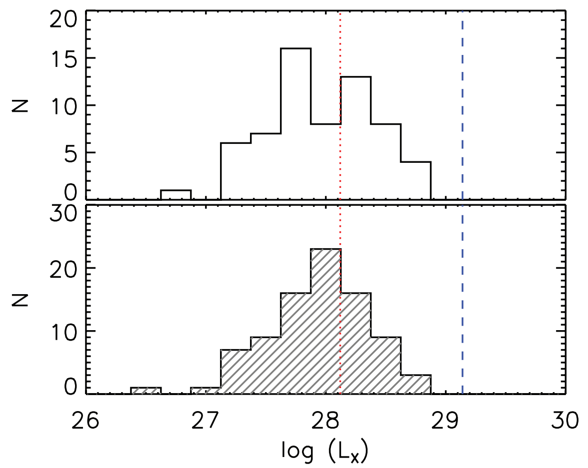

Figure 3. Histogram of the RASS detection limits for the targets within the X-ray (white histogram) and control (grey histogram) samples. Mean L_x values for Pleiades (100 Myr) and Hyades (650 Myr) M dwarfs are shown as blue dashed and red dotted lines, respectively (Stern, Schmitt & Kahabka 1995; Micela et al. 1996).

companions and above: 75 per cent of the X-ray sample and 85 per cent of the control sample. Nearly all the RASS observations were sensitive to K-type companions – 87 per cent of the X-ray and 93 per cent of the control sample – and the few remaining targets were sensitive to F- or G-type companions.

The targets within the X-ray-detected sample were chosen based on the presence of a *ROSAT* BSC (Voges et al. 1999) or *ROSAT* Faint Source Catalogue (FSC; Voges et al. 2000) source within 35 arcsec of the *Hipparcos* coordinate of each target. As noted in Table 5, 51 per cent are from the FSC. Previous correlations between BSC sources and optical star catalogues (e.g. Huensch et al. 1998a) have typically used a maximum offset of 90 arcsec between the catalogue positions to define an X-ray source. The distribution of the offsets between X-ray source position and *Hipparcos* position is given in Fig. 5, and we have applied a more stringent maximum offset cut-off than previous studies, 35 arcsec. All of the A-type stars within the

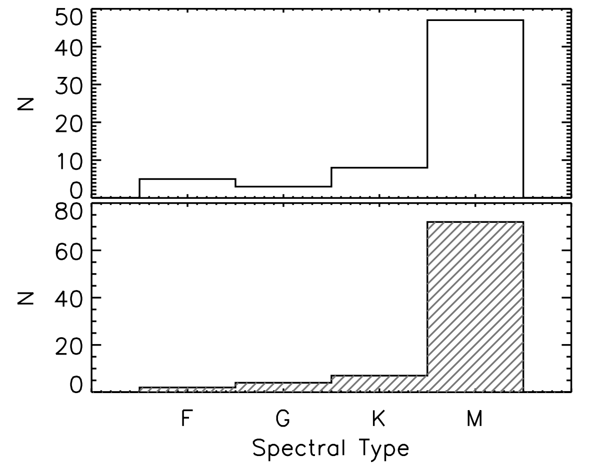

Figure 4. Histogram showing the distribution of the sensitivity of RASS observations to lower mass companions for targets in the X-ray (white histogram) and control (grey histogram) samples. The evolution of L_X as a function of stellar age was derived from observations of open clusters (Güdel 2004, and references therein).

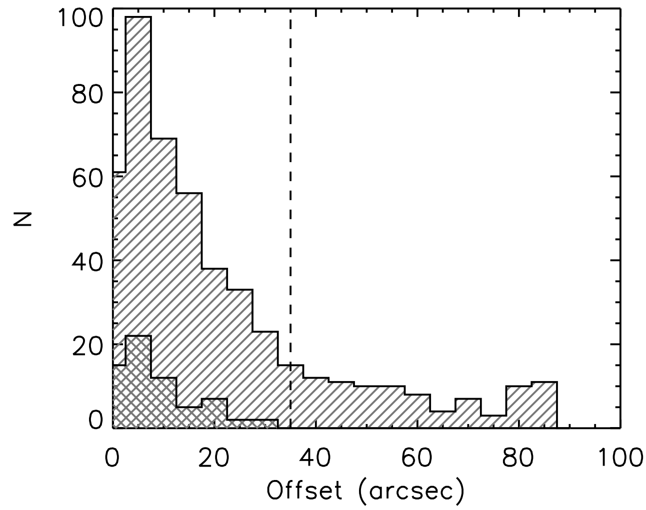

Figure 5. Distribution of *Hipparcos* – *ROSAT* offsets for 479 X-ray detected early-type stars (hatched histogram). These stars have a *ROSAT* source within 90 arcsec using the same criteria as Huensch, Schmitt & Voges (1998a). The tail of the distribution was removed by selecting a more stringent maximum offset of 35 arcsec (dashed line). The offset distribution for the 63 early-type stars within the X-ray detected sample is overplotted (cross-hatched histogram).

X-ray sample were also identified as X-ray stars in previous studies of X-ray-detected A-type stars (e.g. Schröder & Schmitt 2007).

4 OBSERVATIONS

High-resolution AO images were obtained for all 148 stars in order to compare the binary statistics of the X-ray and control samples. The data were acquired with several instruments listed in Table 3 – VisIm (Roberts & Neyman 2002) on AEOS, KIR (Doyon et al. 1998) on Canada–France–Hawaii Telescope (CFHT), NIRI (Hodapp et al. 2003) on Gemini-North and PHARO (Hayward et al. 2001) on Palomar. The resolution limit λ/D ranged from 0.05 arcsec for the I_C-band AEOS images to 0.13 arcsec for the K' CFHT images. The filter used for observations with each instrument is given in Table 3, alongside the corresponding narrow-band filter in parentheses. The full width at half-maximum (FWHM) of the image cores typically matched the diffraction limit, due to the high-quality AO correction on these bright stars. Given the nearby distances of the targets ($D < 170$ pc), the resolution limit corresponds to projected separations of ∼10–20 au. The field of view ranges from 21.7 × 21.7 to 35.6 × 35.6 arcsec^2, making binary systems as wide as ∼3000 au detectable. The effective field of view for the combined science images was increased by dithering the target on the detector. The search range covers the peak of the binary separation distribution of lower mass stars (e.g. Duquennoy & Mayor 1991; Fischer & Marcy 1992), important for resolving the bulk of the binary population.

The observing strategy was consistent for all targets. To search for close companions, unsaturated exposures of each target were obtained using either a narrow-band or a neutral-density filter. Exposure times ranged from 0.01 to 4.0 s, with stacks of three to 500 frames. To detect wider, fainter objects approaching the bottom of the main sequence, longer exposures in a wide-band filter were recorded with total integration times ranging from 41 to 720 s. Details of the filter combinations are given in Table 3 and exposure times of individual targets are listed in Tables 1 and 2. Because of the brightness of the targets, all-sky survey images from Two Micron All Sky Survey (2MASS) are saturated over a significant fraction of the separation range covered by the images within this study.

5 DATA ANALYSIS

The science images were processed with standard image reduction steps including dark subtraction, flat-fielding, interpolation over bad pixels and sky subtraction. Alignment of short-exposure images was achieved through Gaussian centroiding, while the saturated exposures were aligned by cross-correlating the diffraction spikes (e.g. Lafrenière et al. 2007). To improve the measurable contrast ratios, a radial subtraction was performed on the saturated images to suppress the seeing halo of the central star. Finally, all the processed images were median-combined to increase the signal-to-noise ratio of any detection.

Candidates were identified by visual inspection, and the separation and magnitude difference were measured for each candidate, as reported in Tables 4 and 5. The projected separation between the central star and candidate was calculated from the positions of the centroids of each component in the final median-combined image. The uncertainty of the separation incorporates both the uncertainty in the instrument pixel scale, given in Table 3, and the standard deviation of the measurements from each individual exposure. An estimate of the physical separation in au was then determined from the *Hipparcos*-derived distance to the primary. The position angle of each candidate was measured based on the instrument field orientation, given in Table 3, and the rotation angle on the sky for all Gemini and a subset of the AEOS data. For data obtained at Palomar and CFHT, there is no instrument or sky

Table 1. X-ray-detected sample.

HIP	Name	*Hipparcos* spectral type	Distance (pc)	*ROSAT* source Designation B – BSC, F – FSC	Offset (arcsec)	Error radius (arcsec)	Observations Tel.	Date	Magnitude	Band	Integration (s)	2MASS sources arcmin^{-2}
5310	ψ^2 Psc	A3V	49.4 ± 2.0	B – J010757.4+204424	4.9	14	Gemini	16/10/2008	5.22 ± 0.02	*K*	200	0.156
9480	48 Cas	A3IV	35.8 ± 0.7	B – J020156.9+705432	7.6	8	CFHT	01/09/2009	4.25 ± 0.27	*K*	480	0.868
11569	ι Cas	A5p	43.4 ± 1.5	B – J022902.9+672407	6.4	8	CFHT	05/02/2010	4.25 ± 0.03	*K*	330	1.088
13133	RZ Cas	A3Vv+	62.5 ± 2.4	B – J024854.7+693804	4.3	7	Gemini	14/11/2008	5.47 ± 0.02	*K*	400	0.767
17608	Merope	B6IVe	110.1 ± 12.6	F – J034620.7+235713	24.5	13	AEOS	04/02/2002	4.14 ± 0.03	*I*	300	0.207
17664		B9.5V	150.1 ± 22.3	F – J034659.4+243049	23.5	23	AEOS	02/03/2003	6.79 ± 0.01	*I*	599	0.216
17923		A0V	158.7 ± 36.8	B – J034958.2+235109	13.8	14	AEOS	03/02/2002	6.74 ± 0.01	*I*	289	0.212
19949		A2Vn	108.2 ± 8.8	F – J041642.9+533649	6.7	16	AEOS	05/02/2002	5.15 ± 0.00	*I*	300	0.749
20070	b Per	A2V	97.6 ± 8.3	B – J041814.8+501747	3.7	7	AEOS	05/02/2002	4.44 ± 0.03	*I*	300	0.800
20156		A7V	79.4 ± 5.3	B – J041913.6+500254	3.6	8	AEOS	05/02/2002	5.23 ± 0.01	*I*	300	0.781
20380		A3V	95.0 ± 6.1	F – J042149.8+563020	16.8	27	AEOS	05/02/2002	5.79 ± 0.00	*I*	300	0.677
20400	60 Tau	A3m	45.7 ± 2.0	F – J042204.5+140440	14.7	27	AEOS	04/02/2002	5.38 ± 0.03	*I*	300	0.150
20484	63 Tau	A1m	47.2 ± 1.8	F – J042325.5+164633	8.1	28	AEOS	04/02/2002	5.33 ± 0.03	*I*	300	0.180
20648	δ^3 Tau	A2IV	45.3 ± 1.6	F – J042528.4+175512	31.8	14	AEOS	04/02/2002	4.24 ± 0.03	*I*	300	0.189
							CFHT	04/02/2010	4.10 ± 0.03	*K*	352	0.317
21402	88 Tau	A5m	46.1 ± 1.7	B – J043538.5+100941	11.6	8	AEOS	04/02/2002	4.06 ± 0.02	*I*	300	0.171
22287	4 Cam	A3m	49.7 ± 2.0	F – J044758.6+564531	14.6	18	AEOS	05/02/2002	5.08 ± 0.03	*I*	300	0.506
23040	7 Cam	A1V	115.2 ± 10.8	B – J045714.3+534442	34.8	10	AEOS	05/02/2002	4.39 ± 0.03	*I*	300	0.545
23179	ω Aur	A1V	48.8 ± 2.2	B – J045915.4+375330	5.2	7	Gemini	15/11/2008	4.92 ± 0.03	*K*	200	1.125
23875	β Eri	A4III	27.2 ± 0.6	B – J050750.5-050455	17.3	10	Gemini	19/12/2009	2.40 ± 0.22	*K*	200	0.274
24019		A5m	54.7 ± 3.9	F – J050945.2+280209	20	12	AEOS	04/02/2002	5.69 ± 0.01	*I*	300	0.466
26126	38 Ori	A2V	105.8 ± 8.3	F – J053416.4+034623	23.4	17	AEOS	05/02/2002	5.25 ± 0.03	*I*	300	0.322
28614	μ Ori	A1Vm	46.5 ± 1.8	B – J060222.9+093854	4.6	9	Gemini	19/12/2009	3.64 ± 0.26	*K*	200	0.995
29997		A0Vn	53.9 ± 1.9	F – J061849.6+691929	18.7	14	CFHT	01/09/2009	4.67 ± 0.02	*K*	480	0.310
30060	2 Lyn	A2Vs	45.7 ± 2.0	F – J061938.6+590019	22.4	20	AEOS	05/02/2002	4.40 ± 0.00	*I*	300	0.243
							CFHT	01/09/2009	4.35 ± 0.02	*K*	480	0.364
30419	ϵ Mon	A5IV	39.4 ± 1.6	B – J062346.2+043544	9.9	10	CFHT	01/09/2009	3.92 ± 0.04	*K*	480	1.133
35643		A7s	34.5 ± 0.9	F – J072119.0+451327	20.9	22	AEOS	02/02/2002	5.38 ± 0.01	*I*	300	0.183
39095		A1V	73.1 ± 4.3	F – J075951.6-182353	7.4	17	AEOS	02/02/2002	4.51 ± 0.02	*I*	300	0.756
39847	27 Lyn	A2V	66.8 ± 3.1	F – J080828.5+513040	19.3	16	AEOS	02/02/2002	4.71 ± 0.04	*I*	300	0.126
41564		A5m	85.2 ± 6.8	B – J082828.5-023051	13.9	9	AEOS	03/02/2002	6.06 ± 0.01	*I*	300	0.235
42313	δ Hya	A1Vnn	54.9 ± 2.7	B – J083740.1+054217	11.2	11	AEOS	04/02/2002	4.12 ± 0.02	*I*	300	0.166
							AEOS	01/03/2003	4.12 ± 0.02	*I*	300	0.166

Table 1 – *continued*

HIP	Name	*Hipparcos* spectral type	Distance (pc)	*ROSAT* source Designation B – BSC, F – FSC	Offset (arcsec)	Error radius (arcsec)	Observations Tel.	Date	Magnitude	Band	Integration (s)	2MASS sources $arcmin^{-2}$
44127	ι Uma	A7V	14.6 ± 0.2	B – J085913.0+480227	5.9	11	Palomar	12/04/2008	2.66 ± 0.24	*K*	71	0.145
							CFHT	05/02/2010	2.66 ± 0.24	*K*	352	0.145
45688	38 Lyn	A3V	37.4 ± 1.1	B – J091850.2+364814	7.5	8	AEOS	06/02/2002	3.81 ± 0.03	*I*	300	0.081
							Palomar	12/04/2008	3.42 ± 0.35	*K*	71	0.124
51200		A2V	66.3 ± 3.1	F – J102728.3+413613	9.7	13	CFHT	04/02/2010	5.53 ± 0.02	*K*	440	0.104
52913	40 Sex	A2IV	95.9 ± 10.8	F – J104917.1-040123	4.7	14	AEOS	02/03/2003	6.38 ± 0.01	*I*	300	0.083
57646		A3m	62.7 ± 3.2	F – J114915.1+161430	6.4	12	AEOS	02/03/2003	5.75 ± 0.01	*I*	300	0.058
							CFHT	05/02/2010	5.35 ± 0.02	*K*	352	0.091
58001	Phecda	A0Ve	25.6 ± 0.4	B – J115352.3+534153	25	16	Palomar	11/04/2008	2.49 ± 0.17	*H*	71	0.090
							CFHT	05/02/2010	2.43 ± 0.29	*K*	352	0.102
59504		A5m	33.7 ± 0.6	B – J121210.1+773702	7.3	20	AEOS	29/05/2002	4.77 ± 0.00	*I*	300	0.103
62394	34 Vir	A3V	74.6 ± 5.2	F – J124714.4+115723	12.5	19	AEOS	29/05/2002	5.98 ± 0.00	*I*	300	0.059
62572		A1IIIshe	93.0 ± 15.1	F – J124909.8+832448	6.7	13	AEOS	29/05/2002	5.26 ± 0.00	*I*	300	0.126
65198		A2V	65.3 ± 3.4	B – J132141.7+020521	7.2	8	AEOS	02/03/2003	5.64 ± 0.00	*I*	300	0.075
							CFHT	13/06/2008	5.60 ± 0.05	*H*	450	0.103
							CFHT	04/02/2010	5.51 ± 0.02	*K*	440	0.115
65241	64 Vir	A2m	63.7 ± 2.9	B – J132209.8+050918	2.6	10	AEOS	03/03/2003	5.82 ± 0.03	*I*	319	0.066
							CFHT	14/06/2008	5.67 ± 0.03	*H*	450	0.094
65477	Alcor	A5V	24.9 ± 0.3	F – J132513.8+545920	3.9	13	Palomar	11/04/2008	3.30 ± 0.23	*H*	71	0.100
66249	ζ Vir	A3V	22.5 ± 0.4	F – J133442.6-003530	19.6	14	AEOS	03/03/2003	3.27 ± 0.02	*I*	300	0.079
							CFHT	05/02/2010	3.22 ± 0.27	*K*	352	0.122
66727	1 Boo	A1V	92.8 ± 7.8	B – J134040.2+195708	12.8	11	AEOS	03/03/2003	5.72 ± 0.01	*I*	300	0.064
71618	33 Boo	A1V	60.4 ± 2.0	B – J143850.0+442418	3.7	7	CFHT	14/06/2008	5.28 ± 0.04	*H*	450	0.098
76376		A2V	75.5 ± 3.0	B – J153556.8+54375	3.3	9	AEOS	29/05/2002	5.72 ± 0.00	*I*	300	0.089
76878	τ^7 Ser	A2m	53.2 ± 2.3	B – J154154.9+182744	6.9	15	AEOS	29/05/2002	5.61 ± 0.03	*I*	300	0.096
					6.9	15	Palomar	13/07/2008	5.30 ± 0.02	*K*	62	0.149
77336	υ Ser	A3V	77.2 ± 6.0	F – J154717.7+140652	7.3	16	AEOS	29/05/2002	5.61 ± 0.00	*I*	300	0.108
80628	υ Oph	A3m	37.5 ± 1.2	B – J162748.2-082213	4.8	9	Palomar	12/04/2008	4.17 ± 0.04	*K*	47	0.401
82321	52 Her	A2Vspe	53.7 ± 1.5	F – J164914.1+455848	12	12	Palomar	12/07/2008	4.58 ± 0.04	*H*	71	0.174
83223		A7V	73.1 ± 4.6	F – J170028.6+063456	13.4	29	AEOS	29/05/2002	6.33 ± 0.01	*I*	300	0.232
85829	ν^2 Dra	A4m	30.6 ± 0.5	F – J173216.1+551023	1	15	Palomar	12/04/2008	4.16 ± 0.02	*K*	71	0.203
							CFHT	05/02/2010	4.16 ± 0.02	*K*	264	0.223
87045		A2Vs	131.6 ± 14.2	B – J174707.6+473648	5.2	8	AEOS	29/05/2002	6.37 ± 0.01	*I*	300	0.183
87212	30 Dra	A2V	66.5 ± 2.1	F – J174904.5+504651	2.6	34	Gemini	24/06/2008	4.88 ± 0.02	*K*	200	0.259
							Palomar	12/07/2008	4.88 ± 0.02	*K*	71	0.259
88771	72 Oph	A4IVs	25.4 ± 0.5	F – J180719.8+093411	26.4	16	Palomar	12/04/2008	3.41 ± 0.19	*K*	71	0.990
							CFHT	05/02/2010	3.41 ± 0.19	*K*	264	0.990
89925	108 Her	A5m	57.6 ± 2.0	F – J182057.4+295146	14.8	12	AEOS	31/05/2002	5.37 ± 0.03	*I*	300	0.348
							Gemini	24/06/2008	4.99 ± 0.02	*K*	200	0.540
							CFHT	01/09/2009	4.99 ± 0.02	*K*	720	0.540
91971	ζ^1 Lyr	Am	47.1 ± 1.2	B – J184446.1+373620	3.7	9	CFHT	13/06/2008	3.97 ± 0.23	*K*	180	0.566
93747	ζ Aql	A0Vn	25.5 ± 0.5	B – J190526.0+135136	22.8	12	CFHT	13/06/2008	3.05 ± 0.28	*H*	180	5.932
98103	ϕ Aql	A1IV	63.1 ± 3.0	F – J195613.8+112526	8.5	13	Gemini	18/06/2008	5.26 ± 0.02	*K*	200	1.778
102033		A2V	82.0 ± 4.4	F – J204036.8+294822	6.1	15	AEOS	31/05/2002	5.87 ± 0.00	*I*	300	0.993
106711	74 Cyg	A5V	63.3 ± 2.5	F – J213656.7+402440	8.9	14	Gemini	08/09/2008	4.51 ± 0.02	*K*	200	1.218
109521		A5V	54.8 ± 1.7	B – J221109.0+504929	8.7	14	Gemini	08/09/2008	4.96 ± 0.02	*K*	200	2.059
110787	ρ^1 Cep	A2m	62.6 ± 2.0	F – J22264.9+784709	4.5	12	Gemini	17/08/2008	5.54 ± 0.03	*K*	200	0.435
117452	δ Scl	A0V	44.0 ± 2.2	B – J234854.7-280751	11.2	13	CFHT	30/08/2009	4.53 ± 0.02	*K*	480	0.112

rotation. Typically, the total uncertainty is dominated by the measurement uncertainty; however, the lack of calibration measurements within some of the observation runs requires a more conservative estimate of the plate scale and angle of true north uncertainty.

The magnitude difference between each candidate and target star was measured with aperture photometry. Using an aperture of twice the FWHM, the fluxes for the candidate and unsaturated star were measured. If the candidate was only detected in the saturated image, then the comparison flux of the central star was scaled according to the exposure time of the saturated image and the appropriate filter bandpass. The reported magnitude difference uncertainty was estimated as the standard deviation of the values from each processed image before combination. Using the magnitudes of the target from the *Hipparcos* and 2MASS (Skrutskie et al. 2006) source catalogues, the apparent magnitude of the candidate was determined. An estimate of the physical properties of both primary and candidate companion was made using a combined set of theoretical solar metallicity isochrones (Baraffe et al. 1998; Marigo et al. 2008). Each target was plotted on a colour–magnitude diagram (Fig. 2) from which an estimate of the age was derived. Estimated colours and bolometric luminosities were obtained for the companion candidates based on the measured magnitude difference, using an isochrone of the same age as the primary.

Table 2. Control sample.

HIP	Name	*Hipparcos* spectral type	Distance (pc)	Observations Tel.	Date	Magnitude	Band	Integration (s)	2MASS sources (arcmin^{-2})
159		A3	59.1 ± 2.8	Gemini	17/10/2008	6.21 ± 0.02	*K*	200	0.115
2852		A5m	49.7 ± 2.2	Gemini	17/10/2008	5.42 ± 0.02	*K*	200	0.100
3414	π Cas	A5V	53.5 ± 2.1	AEOS	02/03/2003	4.79 ± 0.01	*I*	300	0.334
				Gemini	16/10/2008	4.58 ± 0.02	*K*	200	0.505
5317	41 And	A3m	60.2 ± 2.7	Gemini	16/10/2008	4.77 ± 0.02	*K*	200	0.404
8122		A3	71.7 ± 3.8	CFHT	30/08/2009	6.17 ± 0.02	*K*	640	0.229
9487	α Psc	A2	42.6 ± 1.9	CFHT	01/09/2009	3.62 ± 0.33	*K*	480	0.115
13717		A1Vn	57.9 ± 3.1	Gemini	18/10/2008	4.86 ± 0.02	*K*	200	0.115
17489	Celeno	B7IV	102.6 ± 11.1	AEOS	03/02/2002	5.43 ± 0.03	*I*	300	0.207
17572		A0V	103.3 ± 11.0	AEOS	04/02/2002	6.77 ± 0.01	*I*	300	0.192
17588	22 Tau	A0Vn	108.6 ± 10.9	AEOS	02/02/2002	6.41 ± 0.03	*I*	300	0.213
17791		A1V	144.9 ± 20.8	AEOS	04/02/2002	6.83 ± 0.02	*I*	300	0.217
17847	Atlas	B8III	116.7 ± 14.0	AEOS	04/02/2002	3.64 ± 0.03	*I*	300	0.214
20507	ξ Eri	A2V	63.9 ± 3.3	Gemini	17/10/2008	4.93 ± 0.02	*K*	200	0.187
20641	κ^2 Tau	A7	44.2 ± 1.6	CFHT	05/02/2010	4.61 ± 0.02	*K*	352	0.362
20894	θ^2 Tau	A7III	45.7 ± 1.7	CFHT	04/02/2010	2.88 ± 0.26	*K*	440	0.307
21039	81 Tau	Am	44.3 ± 2.1	CFHT	05/02/2010	4.90 ± 0.02	*K*	352	0.311
22192	EX Eri	A3IV	57.5 ± 2.2	Gemini	14/11/2008	5.72 ± 0.02	*K*	200	0.172
23554		A2IV	60.1 ± 2.3	Gemini	19/12/2009	5.34 ± 0.02	*K*	200	0.209
23983	16 Ori	A2m	53.9 ± 2.4	Gemini	05/11/2008	4.86 ± 0.02	*K*	200	0.403
25197	16 Cam	A0Vne	104.3 ± 8.4	AEOS	05/02/2002	5.23 ± 0.00	*I*	300	0.337
26309		A2III-IV	56.6 ± 2.3	Gemini	14/11/2008	5.86 ± 0.02	*K*	200	0.255
28360	Menkalinan	A2IV+	25.2 ± 0.5	CFHT	05/02/2010	1.78 ± 0.19	*K*	352	0.651
28910	θ Lep	A0V	52.2 ± 1.9	Gemini	25/11/2008	4.52 ± 0.02	*K*	200	0.472
29711		A5IVs	66.5 ± 3.4	Gemini	25/11/2008	5.86 ± 0.02	*K*	200	0.729
31119		A3V	64.8 ± 3.6	AEOS	04/02/2002	5.04 ± 0.01	*I*	300	0.706
				Gemini	11/11/2008	4.77 ± 0.04	*K*	200	1.198
31290		A3V	136.1 ± 18.0	AEOS	05/02/2002	6.46 ± 0.01	*I*	300	0.402
34897		A5	66.4 ± 3.4	Gemini	10/05/2010	5.99 ± 0.02	*K*	200	0.293
35341	65 Aur	A5Vn	82.1 ± 6.2	AEOS	02/02/2002	5.69 ± 0.01	*I*	300	0.207
35350	λ Gem	A3V	28.9 ± 0.8	Palomar	12/04/2008	3.54 ± 0.26	*K*	68	0.489
				CFHT	04/02/2010	3.54 ± 0.26	*K*	440	0.489
38723		A3p	60.4 ± 3.4	Gemini	11/11/2008	5.40 ± 0.02	*K*	200	0.241
40646	29 Lyn	A7IV	93.2 ± 5.9	AEOS	03/02/2002	5.46 ± 0.00	*I*	300	0.116
41152		A3V	51.4 ± 1.9	AEOS	06/02/2002	5.39 ± 0.01	*I*	300	0.113
42806	Asellus Borealis	A1IV	48.6 ± 2.0	AEOS	02/03/2002	4.64 ± 0.00	*I*	300	0.123
43570		A5V	167.8 ± 38.8	AEOS	04/02/2002	6.21 ± 0.01	*I*	300	0.138
43932	σ^2 Cnc	A7IV	59.8 ± 3.3	AEOS	06/02/2002	5.26 ± 0.01	*I*	300	0.099
44066	α Cnc	A5m	53.2 ± 2.8	AEOS	01/03/2003	4.13 ± 0.03	*I*	300	0.119
44901	15 UMa	A1m	29.3 ± 0.7	AEOS	01/03/2003	4.19 ± 0.03	*I*	300	0.087
				Palomar	12/04/2008	4.04 ± 0.28	*K*	69	0.138
				CFHT	05/02/2010	4.04 ± 0.28	*K*	352	0.138
45493	18 UMa	A5V	36.3 ± 1.0	AEOS	03/03/2003	4.58 ± 0.03	*I*	300	0.094
				Palomar	12/04/2008	4.29 ± 0.02	*K*	85	0.138
49593	21 LMi	A7V	28.0 ± 0.7	Palomar	12/04/2008	4.00 ± 0.04	*K*	44	0.108
51658		A7IV	34.3 ± 0.9	Palomar	12/04/2008	4.20 ± 0.02	*K*	69	0.106
				CFHT	04/02/2010	4.20 ± 0.02	*K*	440	0.106
53910	Merak	A1V	24.4 ± 0.4	CFHT	04/02/2010	2.29 ± 0.24	*K*	440	0.106
53954	60 Leo	A1m	37.9 ± 1.2	Palomar	12/04/2008	4.32 ± 0.04	*K*	71	0.103
54063		A5	61.8 ± 3.3	CFHT	14/06/2008	6.29 ± 0.02	*H*	450	0.079
54136	51 UMa	A3III-IV	80.6 ± 4.6	AEOS	03/03/2003	5.86 ± 0.01	*I*	300	0.065
57328	ξ Vir	A4V	36.6 ± 1.1	AEOS	03/03/2003	4.67 ± 0.00	*I*	300	0.067
				Palomar	11/04/2008	4.41 ± 0.05	*K*	71	0.104
				CFHT	13/06/2008	4.54 ± 0.08	*H*	180	0.091
57632	β Leo	A3V	11.1 ± 0.1	CFHT	05/02/2010	1.88 ± 0.19	*K*	352	0.099
58510	7 Vir	A1V	84.8 ± 5.4	AEOS	02/03/2003	5.34 ± 0.00	*I*	290	0.068
58590	π Vir	A5V	109.2 ± 10.1	AEOS	02/03/2003	4.53 ± 0.02	*I*	300	0.067
59394	3 Crv	A1V	56.1 ± 2.1	CFHT	14/06/2008	5.36 ± 0.04	*H*	450	0.165
59608	12 Vir	A2m	49.5 ± 1.8	AEOS	03/03/2003	5.61 ± 0.03	*I*	200	0.060
				CFHT	04/02/2010	5.24 ± 0.02	*K*	440	0.097
59774	Megrez	A3V	25.0 ± 0.4	Palomar	11/04/2008	3.31 ± 0.25	*H*	71	0.094
				CFHT	13/06/2008	3.31 ± 0.25	*H*	180	0.094

Table 2 – *continued*

HIP	Name	*Hipparcos* spectral type	Distance (pc)	Observations Tel.	Date	Magnitude	Band	Integration (s)	2MASS sources ($arcmin^{-2}$)
60746	16 Com	A4V	86.5 ± 5.6	AEOS	03/02/2003	4.93 ± 0.03	*I*	300	0.058
61960	ρ Vir	A0V	36.9 ± 1.1	AEOS	02/03/2003	4.80 ± 0.03	*I*	300	0.064
				Palomar	11/04/2008	4.76 ± 0.02	*H*	57	0.092
				CFHT	04/02/2010	4.68 ± 0.02	*K*	440	1.040
62933	41 Vir	A7III	61.0 ± 2.9	CFHT	05/02/2010	5.47 ± 0.02	*K*	352	0.097
68520	τ Vir	A3V	66.9 ± 3.9	AEOS	03/03/2003	4.11 ± 0.02	*I*	300	0.075
69592		A7V	59.0 ± 2.6	Palomar	12/07/2008	5.90 ± 0.02	*H*	71	0.093
69732	λ Boo	A0p	29.8 ± 0.5	AEOS	03/03/2003	4.15 ± 0.03	*I*	300	0.069
				Palomar	11/04/2008	4.03 ± 0.25	*H*	71	0.095
69951		A5	73.5 ± 3.4	Palomar	12/07/2008	6.40 ± 0.04	*H*	71	0.097
69974	λ Vir	A1V	57.2 ± 3.1	AEOS	03/03/2003	4.43 ± 0.02	*I*	669	0.114
				Gemini	24/06/2008	4.24 ± 0.02	*K*	200	0.177
71075	γ Boo	A7III	26.1 ± 0.5	Palomar	11/04/2008	2.57 ± 0.25	*H*	71	0.089
75043		A4V	65.3 ± 2.2	AEOS	29/05/2002	5.52 ± 0.00	*I*	300	0.082
76852	ι Ser	A1V	58.9 ± 2.7	Palomar	13/07/2008	4.31 ± 0.02	*K*	71	0.142
77233	β Ser	A3V	46.9 ± 1.9	Palomar	12/04/2008	3.55 ± 0.32	*K*	67	0.161
77464		A5IV	49.2 ± 1.7	Gemini	27/06/2008	5.26 ± 0.02	*K*	200	0.238
77622	ϵ Ser	A2m	21.6 ± 0.3	Palomar	12/04/2007	3.43 ± 0.27	*K*	71	0.203
83613	60 Her	A4IV	44.1 ± 1.4	Palomar	12/04/2008	4.61 ± 0.02	*K*	71	0.347
84012	η Oph	A2IV-V	25.8 ± 0.6	Palomar	12/04/2008	2.34 ± 0.24	*K*	71	1.436
86565	o Ser	A2Va	51.5 ± 2.8	Gemini	28/06/2008	4.11 ± 0.25	*K*	200	3.249
87108	γ Oph	A0V	29.0 ± 0.8	Palomar	12/04/2008	3.62 ± 0.23	*K*	71	0.919
				CFHT	31/08/2009	3.62 ± 0.23	*K*	480	0.919
92161	111 Her	A5III	28.4 ± 0.6	CFHT	13/06/2008	4.08 ± 0.03	*H*	180	1.472
95081	π Dra	A2IIIs	68.9 ± 2.2	Gemini	24/06/2008	4.45 ± 0.02	*K*	200	0.380
				Palomar	12/07/2008	4.58 ± 0.17	*H*	71	0.348
95853	ι^2 Cyg	A5Vn	37.5 ± 0.6	CFHT	12/06/2008	3.69 ± 0.23	*H*	280	0.583
99655	33 Cyg	A3IV-Vn	46.7 ± 1.0	CFHT	14/06/2008	4.17 ± 0.27	*H*	450	0.767
99742	ρ Aql	A2V	47.1 ± 1.7	CFHT	30/08/2009	4.77 ± 0.02	*K*	480	1.353
99770	29 Cyg	A2V	41.0 ± 0.9	CFHT	31/08/2009	4.42 ± 0.02	*K*	480	7.030
100108	36 Cyg	A2V	59.7 ± 1.9	AEOS	31/05/2002	5.51 ± 0.00	*I*	300	2.521
				Gemini	08/09/2009	5.49 ± 0.02	*K*	200	6.666
100526		A2	69.2 ± 2.2	Gemini	08/09/2008	6.20 ± 0.02	*K*	200	1.137
101093	θ Cep	A7III	41.6 ± 0.9	CFHT	30/08/2009	3.72 ± 0.32	*K*	200	0.662
101300		Am	81.1 ± 4.6	AEOS	31/05/2002	6.08 ± 0.01	*I*	300	0.980
101483	η Del	A3IVs	53.0 ± 2.3	Gemini	08/09/2008	5.24 ± 10.00	*K*	200	0.796
105966	35 Vul	A1V	55.7 ± 2.2	Gemini	08/09/2008	5.29 ± 0.02	*K*	200	0.630
109427	θ Peg	A1Va	29.6 ± 0.8	CFHT	14/06/2008	3.39 ± 0.21	*H*	450	0.193
109667		A3V	58.1 ± 2.7	Gemini	10/09/2008	5.74 ± 0.02	*K*	200	0.157
				CFHT	31/08/2009	5.74 ± 0.02	*K*	720	0.157
111169	α Lac	A1V	31.4 ± 0.5	Palomar	12/07/2008	3.87 ± 0.21	*H*	71	1.384
				CFHT	30/08/2009	3.85 ± 0.27	*K*	480	1.516
116354	15 And	A1III	71.6 ± 3.2	Gemini	08/09/2008	5.28 ± 0.02	*K*	200	0.405

Table 3. Instruments.

Telescope	Proposal ID	Dates	*N*	Filter	λ/D (arcsec)	Field of view ($arcsec^2$)	Pixel scale (arcsec)	North (°)
AEOS	–	02-02-2002–03-03-2003	101	I_C	0.05	24.6×24.6	0.048 ± 0.003	0.0 ± 1.0
CFHT	2008A-C22	12-06-2008–14-06-2008	14	*H* (Fe II)	0.09	35.6×35.6	0.035 ± 0.0001	-2.4 ± 0.1
	2008A-C22	13-06-2008–14-06-2008	1	K' ($H2_{1-0}$)	0.13	35.6×35.6	0.035 ± 0.0001	-2.4 ± 0.1
	2009B-C06	30-08-2009–01-09-2009	18	K' ($H2_{1-0}$)	0.13	35.6×35.6	0.035 ± 0.0001	-2.4 ± 0.1
	2010A-C14	04-02-2010–05-02-2010	29	K' ($H2_{1-0}$)	0.13	35.6×35.6	0.035 ± 0.0001	-2.4 ± 0.1
Gemini	GN-2008A-Q-74	18-06-2008–24-06-2008	8	K' (Brγ)	0.06	21.7×21.7	0.021 ± 0.0001	0.5 ± 0.3
	GN-2008B-Q-119	17-08-2008–25-11-2008	26	K' (Brγ)	0.06	21.7×21.7	0.021 ± 0.0001	0.5 ± 0.3
	GN-2009B-Q-120	08-09-2009–19-12-2009	6	K' (Brγ)	0.06	21.7×21.7	0.021 ± 0.0001	0.5 ± 0.3
	GN-2010A-Q-75	10-05-2010	1	K' (Brγ)	0.06	27.7×21.7	0.021 ± 0.0001	0.5 ± 0.3
Palomar	–	11-04-2008–13-07-2008	13	*H* ($CH4_S$)	0.07	25.4×25.4	0.025 ± 0.002	-0.7 ± 0.1
Palomar	–	11-04-2008–13-07-2008	22	K_S (Brγ)	0.09	25.4×25.4	0.025 ± 0.002	-0.7 ± 0.1

Table 4. Candidate binary systems within control sample.

Designation	Separation (arcsec)	Position angle (°)	Magnitude difference	Filter	Observation date
HIP 2852 B[a]	0.93 ± 0.01	260.6 ± 0.3	5.07 ± 0.03	Brγ	17/10/2008
HIP 9487 B	1.83 ± 0.01	266.9 ± 0.2	0.33 ± 0.01	$H2_{1-0}$	01/09/2009
HIP 17572 B	3.4 ± 0.1	333.0 ± 1.0	2.54 ± 0.01	I_C	04/02/2002
HIP 28360 C	13.9 ± 0.3	155.0 ± 0.1	8.5 ± 0.2	K'	05/02/2010
HIP 29711 B	∼4.2	∼239.7	<2.5	K'	25/11/2008
HIP 35350 B	9.7 ± 0.1	33.8 ± 0.1	3.8 ± 0.1	Brγ	12/04/2008
HIP 43570 B	0.66 ± 0.02	310.0 ± 1.0	2.58 ± 0.01	I_C	04/02/2002
HIP 44066 B	10.3 ± 0.3	320.9 ± 1.0	5.5 ± 0.2	I_C	01/03/2003
HIP 44901 B[a]	26.2 ± 0.1	33.9 ± 0.1	6.0 ± 0.1	K'	05/02/2010
HIP 51658 B	16.9 ± 0.04	357.6 ± 0.1	6.0 ± 0.2	K'	04/02/2010
HIP 54136 B	7.7 ± 0.3	110.7 ± 1.0	4.6 ± 0.2	I_C	03/03/2003
HIP 58510 B[a]	3.2 ± 0.1	218.4 ± 1.0	9.2 ± 0.3	I_C	02/03/2003
HIP 68520 Aa[a]	14.4 ± 0.5	41.9 ± 1.0	7.7 ± 0.1	I_C	03/03/2003
HIP 69592 B[a]	4.05 ± 0.03	174.5 ± 0.1	5.1 ± 0.1	$CH4_S$	12/07/2008
HIP 75043 B	0.26 ± 0.01	227.6 ± 2.0	6.0 ± 0.4	I_C	29/05/2002
HIP 84012 B	0.58 ± 0.01	236.0 ± 0.2	0.6 ± 0.1	Brγ	12/04/2008
HIP 95081 B[a]	13.1 ± 0.1	16.9 ± 0.3	8.7 ± 0.1	K'	24/06/2008
HIP 101300 B	0.26 ± 0.01	241.7 ± 1.3	1.0 ± 0.1	I_C	31/05/2002
HIP 109667 B[a]	1.12 ± 0.01	285.2 ± 0.3	4.1 ± 0.1	Brγ	10/09/2008
	1.11 ± 0.01	284.7 ± 0.2	4.2 ± 0.1	$H2_{1-0}$	31/08/2009

[a]Previously unresolved companion candidate.

6 RESULTS

6.1 Detections

Among the 148 targets, a total of 68 candidate companions were imaged around 59 members of the total sample. One-third of the candidate companions, 23 systems, are newly resolved. The binary angular separations range from 0.3 to 26.2 arcsec, and the magnitude differences range from 0.3 to 11.9, corresponding to spectral types of mid-A to late M for associated companions. The measured magnitude difference of the candidates is plotted as a function of separation in Fig. 6. Properties of the companion candidates in the X-ray and control samples are listed in Tables 4 and 5, respectively. Candidate companions are limited to those with less than 5 per cent probability of being a background object, based on the star density analysis described in Section 6.3.

6.2 Detection limits

The sensitivity to companions varies with angular separation from the central star due to the significant residual halo from the bright targets. Detection limits for each image are quantified by determining the flux level in a 5 × 5 pixel aperture that would produce a signal 5σ above the noise within the aperture. The median magnitude difference sensitivity curve for each instrument is plotted in Fig. 6. Since the data were obtained at several wavelengths, the bottom of the main sequence corresponds to a different magnitude difference for each instrument. For an A0 primary, a companion at the bottom of the main sequence would have an absolute magnitude of 14.3 at I_C, 10.5 at H and 10.2 at K_S at an age of 700 Myr. The infrared data obtained at CFHT and Gemini are sensitive to the bottom of the main sequence at separations beyond ∼2 arcsec. The achieved contrast for the Palomar data was less due to the shorter exposure times, and reached a companion mass limit of 0.12–0.2 $M_{\odot}$, depending on the age of the target. The AEOS data have a sensitivity limit to companions ranging from 0.08 to 0.1 $M_{\odot}$. The sensitivity to companions for both the X-ray and control samples is similar, making the difference between the two measured binary frequencies a valid test of the companion hypothesis.

6.3 Probability of chance superpositions

An estimate of the probability of each companion candidate being an optical binary was made based on the local stellar densities for each target, measured from the 2MASS source catalogue. The number of sources within a 2° × 2° box of each target was determined in magnitude bins 1 mag in width from 0 to 14 mag for the J, H and K_S bandpasses. An example plot of this differential source count per area is given in Fig. 7. A power-law fit was applied to the counts such that

$$N = \pi \rho^2 10^{b+am}, \qquad (1)$$

where N is the number of sources within a separation ρ from the target, with an apparent magnitude brighter than m, expressed as a function of the two fit parameters a, the gradient, and b, the intercept. For the I_C-band observations obtained at the AEOS, we have approximated the local stellar density using the J-band 2MASS data. Candidates with $N > 0.05$ were assumed to be a background object and not counted for any aspect of this study – a total of 492 candidates were rejected through this process. To compare the stellar density across the samples, Tables 1 and 2 give the number of objects brighter than the 14th magnitude expected per arcmin^2 in the vicinity of each target. In order to prove physical association of the companion candidates which satisfy this criterion, a second epoch measurement will be required.

7 DISCUSSION

7.1 Multiplicity comparison

The frequency of multiple systems in the X-ray and control sample was determined by two methods. In the first calculation, the

Table 5. Candidate binary systems within X-ray-detected sample.

Designation	Separation (arcsec)	Position angle (°)	Magnitude difference	Filters	Observation date	Estimated $V-I$	Estimated $\log(L_X/L_{Bol})$
5310 B[a,b]	0.36 ± 0.01	175.3 ± 0.3	3.91 ± 0.04	Brγ	16/10/2008	1.98	−3.01
9480 B[b]	0.67 ± 0.01	297.3 ± 0.2	1.18 ± 0.02	$H2_{1-0}$	01/09/2008	0.64	−4.24
11569 B[b]	2.77 ± 0.01	230.0 ± 0.2	1.60 ± 0.02	$H2_{1-0}$	05/02/2010	0.64	−4.32
11569 C	7.22 ± 0.01	115.3 ± 0.1	1.98 ± 0.01	$H2_{1-0}$	05/02/2010	0.75	−4.08
13133 C[a]	∼6.6	∼70.5	<1.9	K'	14/11/2008	0.86	−3.00
13133 D[a,b]	3.87 ± 0.03	229.8 ± 0.3	9.4 ± 0.3	K'	14/11/2008	4.94	1.16
17608 Ab[a]	0.25 ± 0.02	111.0 ± 1.1	4.0 ± 0.4	I_C	04/02/2002	0.54	−4.32
17923 B	3.1 ± 0.1	232.3 ± 1.0	2.66 ± 0.01	I_C	03/02/2002	0.65	−3.29
17923 Ca	9.7 ± 0.3	233.7 ± 1.0	2.8 ± 0.1	I_C	03/02/2002	0.68	−3.23
17923 Cb	10.2 ± 0.3	235.0 ± 1.0	4.5 ± 0.2	I_C	03/02/2002	1.08	−2.52
19949 B[a]	13.5 ± 0.4	146.9 ± 1.0	7.3 ± 0.3	I_C	05/02/2002	1.88	−2.63
20648 B	1.7 ± 0.1	337.9 ± 1.0	3.12 ± 0.02	I_C	04/02/2002	0.80	−4.84
	1.80 ± 0.01	341.4 ± 0.1	2.55 ± 0.01	$H2_{1-0}$	04/02/2010		
22287 Ab[b]	0.46 ± 0.01	41.6 ± 1.2	3.8 ± 0.1	I_C	05/02/2002	1.13	−4.41
22287 B[b]	13.2 ± 0.5	238.7 ± 1.0	5.5 ± 0.2	I_C	05/02/2002	1.82	−3.78
23179 B[b]	∼4.7	∼4.0	<2.6	K'	15/11/2008	1.12	−2.81
24019 B[b]	∼11.2	∼26.1	<2.4	I_C	04/02/2002	0.86	−4.38
28614 BaBb[b]	0.40 ± 0.01	22.1 ± 0.3	1.27 ± 0.01	K'	19/12/2009	0.27	−5.36
29997 B[a]	8.47 ± 0.05	218.1 ± 0.4	6.8 ± 0.1	K'	01/09/2009	2.43	−2.16
30419 B[b]	12.20 ± 0.04	29.0 ± 0.2	1.72 ± 0.03	$H2_{1-0}$	01/09/2009	0.65	−4.95
39095 B[b]	5.3 ± 0.2	65.8 ± 1.0	9.5 ± 0.7	I_C	02/02/2002	2.32	−2.63
39847 Aa[a]	4.6 ± 0.2	114.0 ± 1.0	9.5 ± 0.5	I_C	02/02/2002	2.39	−2.26
42313 Ab[a]	2.6 ± 0.1	265.1 ± 1.0	6.6 ± 0.2	I_C	04/02/2002	1.79	−3.08
	2.6 ± 0.1	262.7 ± 3.1	7.3 ± 0.2	I_C	01/03/2003		
44127 B[b]	2.35 ± 0.02	76.6 ± 0.1	4.22 ± 0.02	Brγ	12/04/2008	2.08	−3.55
	2.40 ± 0.01	78.8 ± 0.1	4.36 ± 0.02	$H2_{1-0}$	05/02/2010		
44127 C[b]	1.94 ± 0.02	79.8 ± 0.1	4.26 ± 0.02	Brγ	12/04/2008	2.09	−3.53
	1.92 ± 0.01	87.2 ± 0.1	4.30 ± 0.02	$H2_{1-0}$	05/02/2010		
45688 B[b]	2.5 ± 0.1	222.6 ± 1.0	1.64 ± 0.03	I_C	06/02/2002	0.48	−4.79
	2.60 ± 0.02	224.0 ± 0.1	1.2 ± 0.1	Brγ	12/04/2008		
51200 B[b]	2.41 ± 0.01	304.1 ± 0.1	3.08 ± 0.01	$H2_{1-0}$	04/02/2010	1.42	−3.63
52913 B[b]	2.3 ± 0.1	13.8 ± 1.1	0.31 ± 0.01	I_C	02/03/2003	0.31	−5.13
62394 Ab[a,b]	3.2 ± 0.1	348.8 ± 1.4	7.0 ± 0.2	I_C	29/05/2002	2.16	−2.37
65241 B[a,b]	0.34 ± 0.02	41.7 ± 3.2	4.3 ± 0.4	I_C	03/03/2003	1.40	−3.16
65477 B[b]	1.07 ± 0.01	209.0 ± 0.1	5.6 ± 0.1	$CH4_S$	11/04/2008	2.19	−3.46
66249 B	1.81 ± 0.01	154.4 ± 0.1	6.4 ± 0.1	$H2_{1-0}$	05/02/2010	2.45	−3.18
66727 B	4.4 ± 0.1	338.5 ± 1.2	2.95 ± 0.02	I_C	03/03/2003	0.74	−3.72
76376 C[a,b]	9.6 ± 0.4	350.1 ± 1.0	11.9 ± 0.3	I_C	29/05/2002	3.6	−1.52
76878 B[b]	2.3 ± 0.1	53.4 ± 1.7	7.3 ± 0.2	I_C	29/05/2002	2.24	−2.31
	2.4 ± 0.02	86.4 ± 0.1	5.1 ± 0.4	K_S	13/07/2008		
80628 B[b]	0.67 ± 0.01	22.6 ± 0.1	2.26 ± 0.03	Brγ	12/04/2008	0.90	−3.78
82321 B	1.82 ± 0.01	34.1 ± 0.1	2.2 ± 0.1	$CH4_S$	12/07/2008	0.77	−4.66
82321 C	2.06 ± 0.02	38.4 ± 0.1	2.69 ± 0.03	$CH4_S$	12/07/2008	0.90	−4.39
87045 B[b]	0.32 ± 0.01	144.1 ± 1.1	2.45 ± 0.04	I_C	29/05/2002	0.62	−3.71
88771 B[b]	24.83 ± 0.06	297.6 ± 0.1	5.2 ± 0.1	K'	05/02/2010	2.18	−3.83
88771 D	24.20 ± 0.06	48.4 ± 0.1	8.1 ± 0.1	K'	05/02/2010	3.40	−2.53
91971 B	23.28 ± 0.07	51.3 ± 0.2	9.7 ± 0.2	K'	13/06/2008	4.27	−0.33
93747 B	7.27 ± 0.02	47.0 ± 0.2	4.88 ± 0.02	Fe II	13/06/2008	1.99	−3.23
98103 C[a,b]	2.8 ± 0.1	184.7 ± 0.2	4.7 ± 0.1	K'	18/06/2008	2.05	−2.96
102033 B[b]	0.72 ± 0.02	345.4 ± 1.1	2.36 ± 0.01	I_C	31/05/2002	0.72	−4.62
106711 B[a]	6.98 ± 0.04	58.1 ± 0.3	8.5 ± 0.1	K'	08/09/2008	3.00	−2.14
109521 B[a,b]	9.98 ± 0.06	241.3 ± 0.3	8.1 ± 0.1	K'	08/09/2008	3.27	−1.18
110787 B[a,b]	0.29 ± 0.01	211.1 ± 0.6	4.3 ± 0.1	Brγ	17/09/2008	2.03	−3.18
117452 Ba[a,b]	3.7 ± 0.1	237.3 ± 0.4	3.48 ± 0.04	$H2_{1-0}$	30/08/2009	1.61	−3.01
117452 Bb[a,b]	3.5 ± 0.1	238.5 ± 0.5	3.7 ± 0.1	$H2_{1-0}$	30/08/2009	1.73	−2.90

[a]Previously unresolved companion candidate.
[b]Companion candidate falls within RASS error ellipse.

total field of view of each observation was used, and, in the second calculation, the search area was restricted to the RASS position error box. For each approach, candidate companions with a small magnitude difference, consistent with a spectral type in the B6–A7 range, were excluded from the X-ray companion hypothesis test and are listed separately in Table 6. This criterion of a companion capable of generating X-rays eliminated one binary companion from the X-ray sample and two companions from

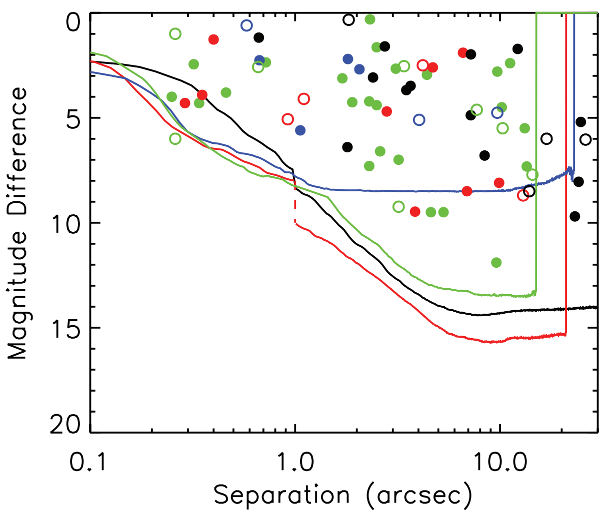

Figure 6. The magnitude difference of the candidate companions detected within this study as a function of angular separation from the central star. Filled and open circles represent companions within the X-ray and control samples, respectively. Colours represent each of the instruments used: AEOS (green); CFHT (black); Gemini (red) and Palomar (blue). Overplotted are the detection limits for each instrument (see Section 6.2). The dashed portion of the Gemini sensitivity curve represents the edge of the field of view for the unsaturated exposures.

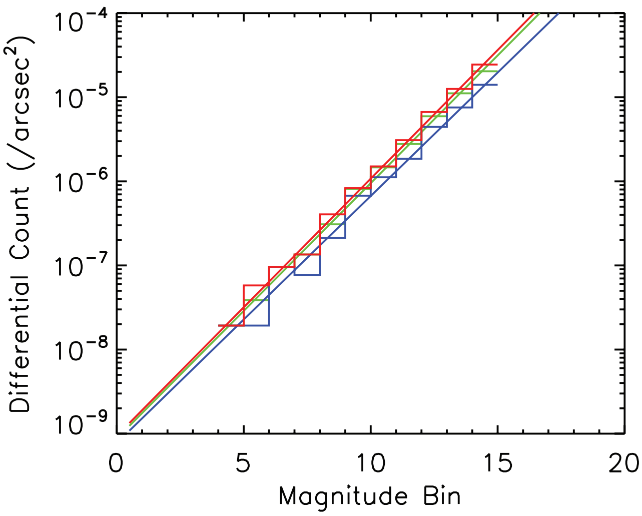

Figure 7. Histogram of differential source counts and corresponding logarithmic fits within the 2MASS source catalogue in the vicinity of HIP 57646 in *J*, *H* and K_S filters (blue, green and red, respectively).

the control sample. All multiple systems considered also satisfied the background object probability of <5 per cent, as described in Section 6.3.

Considering the total field of view of the combined dithered observations, candidates satisfying the magnitude and background probability criteria were included in the multiple frequency measurement. Among the X-ray sample, 60^{+6}_{-6} per cent were multiple, compared to 20^{+5}_{-4} per cent for the control sample – a difference of 40 ± 8 per cent, a 5σ result. These and subsequent reported errors are estimated from a binomial distribution (e.g. Burgasser et al. 2003). Spectroscopic binaries – unresolved with these observations – constitute a significant fraction of both samples (∼15 per cent; Pourbaix et al. 2004). This estimate represents a lower limit on the frequency since the sample of stars observed with the radial velocity monitoring is not known, and the large $v\sin i$ of the primary and less massive unseen companions make such observations challenging. These spectroscopically resolved binaries are not considered within our statistics.

Table 6. Results summary.

	Total field of view X-ray (per cent)	Total field of view Control (per cent)	RASS error ellipse search area X-ray (per cent)	RASS error ellipse search area Control (per cent)
A8–M9 companion[a]	60^{+6}_{-6}	20^{+5}_{-4}	43^{+6}_{-6}	12^{+4}_{-3}
B6–A7 companion	2^{+4}_{-1}	2^{+3}_{-1}	3^{+4}_{-1}	2^{+3}_{-1}
No resolved companion	38^{+6}_{-6}	78^{+4}_{-5}	56^{+6}_{-6}	86^{+3}_{-4}

[a]Expected spectral type based on measured magnitude difference and assuming the same distance as the target.

The multiplicity of the X-ray sample was also measured by considering only companion candidates that were located within the confines of the RASS error ellipse. For each target, the AO data covered a portion of the RASS error ellipse ranging from 25 to 100 per cent. This additional restriction lowered the multiple frequency to 43^{+6}_{-6} per cent. To determine a comparable frequency for the control sample, a series of companion searches were performed by randomly assigning the RASS optical offset and corresponding error ellipse of an X-ray target to a control target and determining the number of candidate companions which fall within the error ellipse. Based on a large number of simulations (100 000), the frequency of multiples was estimated as 12^{+4}_{-3} per cent. These two frequencies are different by 31 ± 7 per cent, a 4σ result.

A summary of the multiplicity calculations is given in Table 6. The high statistical significance of the difference in frequencies for the X-ray and control samples provides strong support of the companion hypothesis as an explanation of the X-ray detection of B6–A7 stars. Further evidence for individual systems with separations of a few arcseconds could be provided by high-resolution *Chandra* observations which would have the pointing accuracy to assign the X-ray flux to the companion unambiguously. One target, Merope in the Pleiades, was observed with the high-resolution mode of *Chandra*, but the binary separation is only 0.25 arcsec, making the discrepancy between the *Chandra* and 2MASS coordinates ambiguous in this case. Targets within the X-ray sample for which no companions have been resolved will make prime targets for future interferometric and spectroscopic study in a search for lower mass companions with angular separations low enough to render them undetectable with AO observations.

7.2 *ROSAT* positional uncertainty

Previous studies of the unexplained X-ray detection of early-type stars (e.g. Schröder & Schmitt 2007) have used the same definition of an X-ray-detected early-type star as presented by Huensch et al. (1998a) – any X-ray source within 90 arcsec of an optical source can be attributed to the optical source. This value was based on estimating the frequency of false attribution by means of a Monte Carlo simulation, and was selected at the radius at which the probability of correctly attributing an X-ray source is ∼50 per cent. A significantly lower offset of 25 arcsec was calculated by Voges et al. (1999) from a correlation of the Tycho catalogue and *ROSAT* BSC positions, a radius within which 90 per cent of the optical targets have an X-ray source attributed. This measurement represents the empirical positional uncertainty of the RASS source catalogue positions.

The sample investigated within this study was initially selected in the same manner as Huensch et al. (1998a) – using a maximum offset of 90 arcsec. The tail of the offset distribution was removed by applying a more stringent maximum offset at 35 arcsec, as described in Section 3. Variations in the field-of-view size between instruments caused the coordinates of the X-ray source given within the RASS to be outside of the field of view within a small subset of the observations. In order to investigate any biases this may have had upon the results presented previously, the sample was further restricted to only include those targets for which the RASS source position was within the field of view and at least 50 per cent of the RASS error ellipse was covered – a total of 45 stars. For this sample, a marginally higher frequency of companions located within the RASS error ellipse was recorded, 53^{+7}_{-7} per cent, reinforcing the result obtained with the unrestricted sample.

7.3 Comparison of measured and expected X-ray luminosities

7.3.1 Candidate companions with measured colours

Several of the candidate companions to X-ray targets have a measured $I-K$ colour from this study, and are plotted in Fig. 8. The colour provides additional information to estimate the spectral type of the object and to test further the capacity of the second object to generate X-ray emission. The three systems with colours are (1) HIP 20648, (2) HIP 45688 and (3) HIP 76878. The $I-K$ colours of the candidate companions are all consistent with X-ray-emitting companions: 0.71 ± 0.05 or late F/early G type for HIP 20648 B, 0.83 ± 0.37 or mid-G type for HIP 45688 B and 2.54 ± 0.44 or late M type for HIP 76878 B.

With the assumption of a distance and age equivalent to the primary distance, the X-ray luminosity associated with the *ROSAT* detection can be checked for consistency with the spectral type. The position on the colour–magnitude diagram for each primary star and its imaged candidate companion is given in Fig. 8, assuming the distance to each component is the same. Each case is

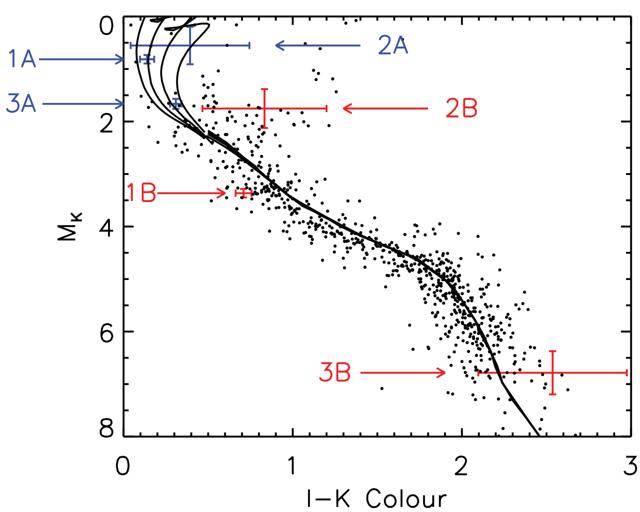

Figure 8. A colour–magnitude diagram of 792 nearby Gliese stars. Overplotted are four theoretical isochrones of ages $\log t = 8.7, 8.8, 8.9, 9.0$ (Baraffe et al. 1998; Marigo et al. 2008). Three of the targets within the X-ray sample are plotted in blue: HIP 20648 (1), HIP 45688 (2) and HIP 76878 (3). The corresponding resolved companions for each primary are shown in red.

examined individually, and the colour and proper motion measurements clearly support the assignment of the X-ray emission to the candidate companion in two cases, while one case remains uncertain.

The theoretical isochrone that best fits the first target, HIP 20648A, corresponds to an age of ∼650 Myr, and the candidate companion position in Fig. 8 is as expected for an associated companion. The companion X-ray luminosity is $\log L_X = 28.71$, and this value falls between the X-ray luminosities of Hyades F- and G-type stars. The assessment of the second target, HIP 45688, is complicated by the presence of a known close companion to the imaged candidate companion ($\rho \sim 0.06$ arcsec; McAlister et al. 1993), unresolved in the current data. The composite colour and magnitude of the BaBb system appear to be more luminous than expected for an object at the 630 Myr age estimated for the primary, even if the pair is an equal-magnitude binary. The X-ray luminosity of BaBb would be $\log L_X = 29.43$, significantly higher than younger G-type stars in the Hyades. For the final system, HIP 76878, the best-fitting age is 700 Myr, similar to the Hyades. The X-ray luminosity of the candidate companion is $\log L_X = 29.26$, if the distance is equal to that of HIP 76878. This X-ray level is higher than the observed X-ray luminosities of M dwarfs of similar age within the Hyades (Stern et al. 1995). In this case, the time baseline between the two observations also reveals a significant motion of the candidate relative to the primary on a trajectory different from both a background object and a bound companion. The presence of a foreground M dwarf in a chance superposition with HIP 76878 explains this discrepant proper motion, the red colour of the object and the unusually high X-ray luminosity.

7.3.2 Candidate companions in open clusters

A subset of the X-ray-detected targets with imaged candidate companions are members of stellar clusters. HIP 17608 and HIP 17923 are Pleiades members, while HIP 20648 is a Hyades member. Extensive X-ray population studies of both the Pleiades (e.g. Micela et al. 1985; Stauffer et al. 1994; Daniel, Linsky & Gagné 2002) and the Hyades (e.g. Micela et al. 1988; Stern et al. 1995) have been conducted with *Einstein*, *ROSAT* and *Chandra*, providing comparison X-ray luminosities to test the likelihood that the candidate companions are responsible for the detected X-ray emission.

The candidate companion to HIP 17608 (Merope in the Pleiades) with a 0.25-arcsec separation is shown in Fig. 9. With a magnitude difference of $\Delta I_C = 4.0 \pm 0.4$, the second object is a mid-F-type star if associated. Assuming a distance to the Pleiades of 133 pc (Pan, Shao & Kulkarni 2004), the X-ray luminosity for the HIP 17608 system is $\log L_X = 29.91$. The typical X-ray luminosity of F dwarfs within the Pleiades is estimated to be $\log L_X \sim 29.43 \pm 0.29$ (Stauffer et al. 1994), indicating that the companion to HIP 17608, if associated, is on the upper limit of X-ray activity for this class of star.

For the second Pleiades member, the observations resolve three of the companions (B, Ca and Cb) within the HIP 17923 quintuple system. Based on the measured magnitude differences, we estimate the mass of the components as follows: B – 1.2 ± 0.1 $M_\odot$ (mid-F type); Ca – 1.2 ± 0.1 $M_\odot$ (mid-F type) and Cb – 0.9 ± 0.1 $M_\odot$ (mid-G type). Deeper X-ray observations of the Pleiades (Micela et al. 1999) revealed an estimated X-ray luminosity of $\log L_X = 30.08$ for this system. If the X-ray counts were distributed evenly between the three later type companions resolved within our AO

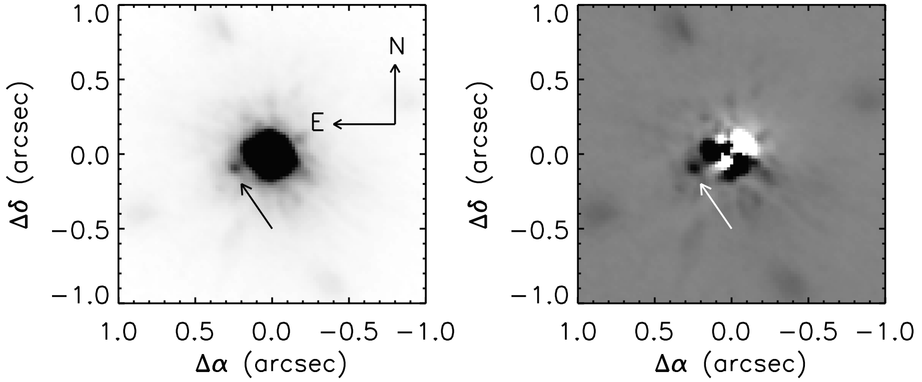

Figure 9. A subarcsecond companion candidate is resolved around HIP 17608 (Merope), a member of the Pleiades cluster. A faint ($\Delta I = 4.0 \pm 0.4$) companion candidate at $\rho = 0.25$ arcsec, $\theta = 110°$ is visible within the median combined image of the 500, 0.048 s unsaturated exposures (left-hand panel). The scale is linear from 0 (white) to 45 (black). After radial subtraction the object becomes more prominent (right-hand panel), with a linear scale between −15 and 20.

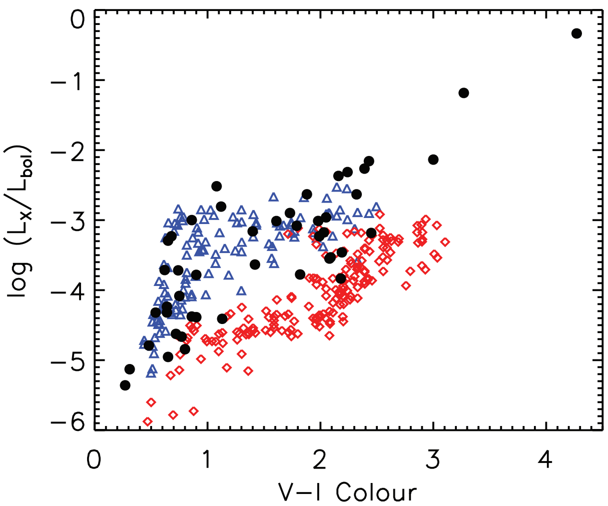

Figure 10. The ratio of X-ray to bolometric luminosity is plotted as a function of colour for the candidates resolved within this study. The majority of candidates are constrained by the Pleiades (blue triangles) and Hyades (red diamonds) members, representing the two age extremes of the sample.

images, the individual X-ray luminosities would be $\log L_X \sim 29.6$, similar to G- and F-type Pleiades members (Stauffer et al. 1994).

The final cluster X-ray target with a resolved companion is the Hyades member HIP 20648. As described in Section 7.2, the candidate companion also has a measured $I - K$ colour consistent with a late F-type/early G-type star, and the X-ray luminosity assigned to the target is consistent with a Hyades G-type star (Stern et al. 1995).

7.3.3 Remaining candidate companions

For the remaining candidate companions, an estimate of the ratio of X-ray to bolometric luminosity can be made under the assumption that the candidate is a physical companion at the same distance. From the absolute magnitude, the $V - I$ colour and bolometric luminosity were inferred from theoretical isochrones (Baraffe et al. 1998). The ratios of the observed X-ray luminosity to the estimated bolometric luminosity (L_X/L_{bol}) are plotted as a function of $V - I$ colour in Fig. 10, with Pleiades and Hyades members (Zuckerman & Song 2004) overplotted as reference populations spanning the age range of the sample.

All but two of the candidates are within the region bound by the ~100 Myr Pleiades and ~650 Myr Hyades members. Uncertainty exists on both axes since both the $V - I$ colour and bolometric luminosity are estimated from theoretical isochrones, assuming the distance. Future observations to accurately determine the colour of these candidates will provide a more robust estimate of the bolometric luminosity. The two outlying candidates shown in Fig. 10 have unphysical high luminosity ratios, significantly higher than the observed luminosity ratios of late M-type stars (e.g. Pizzolato et al. 2003). In these two cases, additional unresolved companions, or background X-ray sources, present a more feasible explanation for the detected X-ray flux. The rate of false detections, 2/49, corresponds to the 5 per cent contamination introduced through the statistical method applied to the candidates to remove background sources, as described in Section 6.3.

8 SUMMARY

In summary, a total of 148 stars with spectral types in the range B6–A7 and distances of <200 pc have been observed with AO-equipped cameras on 3.8–8 m telescopes. The high-resolution images were sensitive to companions with angular separations from ~0.3 to 26.2 arcsec and magnitude differences extending to ~14 mag. A total of 68 candidate companions to 59 targets were resolved, and the frequency of multiple systems was measured to be substantially higher for the X-ray-detected sample. The high frequency of multiples, 43^{+6}_{-6} per cent, compared to 12^{+4}_{-3} per cent for the control sample is different by 4σ and provides strong evidence that the source of the X-ray emission is the candidate companion. The X-ray-detected stars with no resolved companion make ideal candidates for future interferometric observations, as this study has shown that the X-ray detection is indicative of the presence of an unresolved companion, and interferometry can resolve binaries below the resolution of the AO data presented here.

For three candidate companions to X-ray targets, the $I - K$ colour was also measured, and the colours are consistent with late F-type to late M-type stars, supporting the identification of the second object as the X-ray source in two cases. Among the X-ray targets with candidate companions, there are also three cluster members, and the known age, distance and cluster X-ray properties enabled a further test of the companion X-ray luminosity with other cluster members. In each case, the companions – if associated – would have an X-ray luminosity similar to, or on the upper range of, cluster stars with similar magnitude. Follow-up observations of the X-ray targets with candidate companions using *Chandra* would provide the angular resolution in the X-ray band necessary to confirm the second object as the true source of the X-ray emission.

ACKNOWLEDGMENTS

We gratefully acknowledge several sources of funding. RJDR and JB (ST/F 007124/1) are funded through studentships from the Science and Technology Facilities Council (STFC). This work was initiated with a grant awarded to JP from the Air Force Office of Scientific Research (AFOSR) for the AEOS component and completed with a grant from the STFC (ST/F003277/1). Funding for collaborative visits was provided by the CONSTELLATION EC Research Training Network. Portions of this work were performed under the auspices of the US Department of Energy by Lawrence Livermore National Laboratory in part under contract W-7405-Eng-48 and in part under contract DE-AC52-07NA27344, and also supported in part by the National Science Foundation (NSF) Science and Technology CfAO, managed by the UC Santa Cruz under cooperative agreement AST 98-76783. This work was supported, through JRG, in part by University of California Lab Research Programme 09-LR-118057-GRAJ and NSF grant AST-0909188. We thank LLNL summer students C. White (US Air Force Academy) and S. Kost (Carnegie Mellon University) who assisted with obtaining a subset of the data and some of the early analysis. This research has made use of the SIMBAD and VizieR databases, operated at CDS, Strasbourg, France. This publication makes use of data products from the Two Micron All Sky Survey, which is a joint project of the University of Massachusetts and the Infrared Processing and Analysis Center/California Institute of Technology, funded by the National Aeronautics and Space Administration and the NSF. This research has made use of the Washington Double Star Catalogue maintained at the US Naval Observatory. We thank the referee for the helpful comments during the review process.

REFERENCES

Baraffe I., Chabrier G., Allard F., Hauschildt P. H., 1998, A&A, 337, 403
Berghofer T. W., Schmitt J. H. M. M., 1994, A&A, 292, L5
Burgasser A. J., Kirkpatrick J. D., Reid I. N., Brown M. E., Miskey C. L., Gizis J. E., 2003, ApJ, 586, 512
Chabrier G., Baraffe I., 1997, A&A, 327, 1039
Chabrier G., Küker M., 2006, A&A, 446, 1027
Daniel K. J., Linsky J. L., Gagné M., 2002, ApJ, 578, 486
De Pontieu B. et al., 2007, Sci, 318, 1574
Doyon R., Nadeau D., Vallee P., Starr B. M., Cuillandre J. C., Beuzit J.-L., Beigbeder F., Brau-Nogue S., 1998, in Fowler A. M., ed., Proc. SPIE, Vol. 3354, Infrared Astronomical Instrumentation. SPIE, Bellingham p. 760
Duquennoy A., Mayor M., 1991, A&A, 248, 485
ESA, 1997, The Hipparcos and Tycho Catalogues. ESA, SP-1200
Feldmeier A., Puls J., Pauldrach A. W. A., 1997, A&A, 322, 878
Fischer D. A., Marcy G. W., 1992, ApJ, 396, 178
Giampapa M. S., Prosser C. F., Fleming T. A., 1998, ApJ, 501, 624
Güdel M., 2004, A&AR, 12, 71
Hayward T. L., Brandl B., Pirger B., Blacken C., Gull G. E., Schoenwald J., Houck J. R., 2001, PASP, 113, 105
Hinkley S. et al., 2010, ApJ, 712, 421
Hodapp K. W. et al., 2003, PASP, 115, 1388
Hoffleit D., 1969, Catalogue of Bright Stars. Yale Univ. Observatory, New Haven
Hubrig S., Mignant D. L., North P., Krautter J., 2001, A&A, 372, 152
Huélamo N., Neuhäuser R., Stelzer B., Supper R., Zinnecker H., 2000, A&A, 359, 227
Huensch M., Schmitt J. H. M. M., Voges W., 1998a, A&AS, 127, 251
Huensch M., Schmitt J. H. M. M., Voges W., 1998b, A&AS, 132, 155
Jess D. B., Mathioudakis M., Erdélyi R., Crockett P. J., Keenan F. P., Christian D. J., 2009, Sci, 323, 1582
Lafrenière D. et al., 2007, ApJ, 670, 1367
Lucy L. B., White R. L., 1980, ApJ, 241, 300
McAlister H. A., Mason B. D., Hartkopf W. I., Shara M. M., 1993, AJ, 106, 1639
Mamajek E. E., Kenworthy M. A., Hinz P. M., Meyer M. R., 2010, AJ, 139, 919
Marigo P., Girardi L., Bressan A., Groenewegen M. A. T., Silva L., Granato G. L., 2008, A&A, 482, 883
Micela G., Sciortino S., Serio S., Vaiana G. S., Bookbinder J., Golub L., Harnden F. R., Rosner R., 1985, ApJ, 292, 172
Micela G., Sciortino S., Vaiana G. S., Schmitt J. H. M. M., Stern R. A., Harnden F. R., Rosner R., 1988, ApJ, 325, 798
Micela G., Sciortino S., Kashyap V., Harnden F. R., Rosner R., 1996, ApJS, 102, 75
Micela G. et al., 1999, A&A, 341, 751
Owocki S. P., Castor J. I., Rybicki G. B., 1988, ApJ, 335, 914
Pan X., Shao M., Kulkarni S. R., 2004, Nat, 427, 326
Patterson J., Raymond J. C., 1985, ApJ, 292, 535
Pizzolato N., Maggio A., Micela G., Sciortino S., Ventura P., 2003, A&A, 397, 147
Pourbaix D. et al., 2004, A&A, 424, 727
Randich S., 2000, in Pallavicin R., Micela G., Sciortino S., eds, ASP Conf. Ser. Vol. 198, Stellar Clusters and Associations: Convection, Rotation, and Dynamos. Astron. Soc. Pac., San Francisco, p. 401
Roberts L. C., Neyman C. R., 2002, PASP, 114, 1260
Schatzman E., 1949, Ann. Astrophys., 12, 203
Schmitt J. H. M. M., Golub L., Harnden F. R., Maxson C. W., Rosner R., Vaiana G. S., 1985, ApJ, 290, 307
Schmitt J. H. M. M., Micela G., Sciortino S., Vaiana G. S., Harnden F. R., Rosner R., 1990, ApJ, 351, 492
Schmitt J. H. M. M., Zinnecker H., Cruddace R., Harnden F. R., 1993, ApJ, 402, L13
Schröder C., Schmitt J. H. M. M., 2007, A&A, 475, 677
Schwarzschild M., 1948, ApJ, 107, 1
Shapiro S. L., Lightman A. P., Eardley D. M., 1976, ApJ, 204, 187
Shatsky N., Tokovinin A., 2002, A&A, 382, 92
Simon T., Drake S. A., Kim P. D., 1995, PASP, 107, 1034
Skrutskie R. M. et al., 2006, AJ, 131, 1163
Spiegel E. A., Weiss N. O., 1980, Nat, 287, 616
Stauffer J. R., Caillault J.-P., Gagne M., Prosser C. F., Hartmann L. W., 1994, ApJS, 91, 625
Stern R. A., Schmitt J. H. M. M., Kahabka P. T., 1995, ApJ, 448, 683
Sturrock P. A., 1999, ApJ, 521, 451
Topka K., Golub L., Gorenstein P., Harnden F. R., Vaiana G. S., Avni Y., Rosner R., 1982, ApJ, 259, 677
Vaiana G. S. et al., 1981, ApJ, 245, 163
Voges W. et al., 1999, A&A, 349, 389
Voges W. et al., 2000, VizieR On-line Data Catalog, 9029, 0
Zimmerman N. et al., 2010, ApJ, 709, 733
Zuckerman B., Song I., 2004, ARA&A, 42, 685

This paper has been typeset from a TEX/LATEX file prepared by the author.